EasyChair Preprint

№ 10916

Evaluating Grid Support Features of Voltage Source Inverter: an Analysis of Direct Power Control

Chikezie Emeghara, Satish Mahajan, Ali Arzani and Ejikeme Amako

September 18, 2023

Evaluating Grid Support Features of Voltage Source Inverter: An Analysis of Direct Power Control

1st Chikezie M. Emeghara
Dept. of ECE
Tennessee Tech
TN 38501, USA
cmemeghara42@tntech.edu

2nd Satish M. Mahajan
CESR
Tennessee Tech
TN 38501, USA
smahajan@tntech.edu

3rd Ali Arzani
CESR
Tennessee Tech
TN 38501, USA
aarzani@tntech.edu

4th Ejikeme A. Amako
Dept. of ECE
Tennessee Tech
TN 38501, USA
eaamako42@tntech.edu

***Abstract*—This paper provides valuable insights into evaluating voltage source inverter grid support features, emphasizing the importance of direct power control (DPC) in enhancing grid stability, performance, and robustness. The DPC model is designed in a stationary reference frame, eliminating the need for a phase-locked loop, which is required in conventional vector current control methods. It uses simple feed-forward and feedback control loops to ensure proper power injection into the grid. The results indicate that the DPC exhibits a faster dynamic response and is more resilient to changes in grid parasitic elements compared to the classical vector current control model.**

***Index Terms*—Voltage source inverter, Direct power control, grid, short-circuit ratio**

I. Introduction

Grid-connected voltage source inverter (VSI) direct power control (DPC) has emerged as a critical device for seamlessly integrating renewable energy sources and energy storage systems into the power grid. With the growing emphasis on transitioning to a more sustainable and low-carbon energy future, the penetration of distributed generation systems, such as solar photovoltaics, wind turbines, and energy storage systems, has increased [1]. The effective management of power flow between these systems and the grid is of paramount importance to ensure grid stability, power quality, and efficient utilization of renewable resources [2].

In a typical grid-connected renewable generation system, the VSI is the interfacing element between the DC source and the AC grid and is pivotal in maintaining the desired power quality and grid stability [3]. Moreover, with the growing integration of renewable resources into the grid, advanced control techniques for inverters have become crucial to ensure efficient power delivery. Various VSIs control techniques have been proposed, each tailored to specific challenges and scenarios. Methods such as improved linear sinusoidal tracers and notch filter-based control are recognized for their effectiveness in cases of phase imbalance and selective frequency rectification [4] [5]. These techniques may require additional compensation input to achieve optimal power factor control and harmonics reduction.

On the other hand, more complex approaches have been developed, including techniques involving Cauchy–Schwarz inequality theory, synchronous reference frame-based proportional integral control, instantaneous active and reactive current component methods, Kalman filters [6], and notch-filtering techniques [7]. These methods target specific control and compensation application. In addition, the literature has shown a growing interest in adaptive techniques, including intelligent neuro-fuzzy inference [8], combined finite-state and valley current predictive control [9], and decentralized dynamic state estimation [10] [9]. These strategies have shown promising results in computing the phase and amplitude of signals, particularly under distorted grid voltage conditions and, to some extent, during the presence of harmonics but have limited application to the point of common coupling (PCC) under weak grid conditions.

Among the various control methods, vector current control (VCC) and direct power control have emerged as the most widely adopted approaches for power converters [11] [12] [13]. In VCC, the system is modeled in a rotating synchronous reference frame and typically requires the implementation of a phase-locked loop (PLL). Unlike the VCC method, DPC has gained increasing attention recently due to its fast dynamic response, simple control structure, and ability to maintain the required power quality standards [11] [14]. By directly calculating the required switching state of the VSI based on the instantaneous errors in active and reactive power, DPC enables real-time adjustments to the inverter's output, contributing to the grid's robustness [11].

This paper aims to provide an analysis of grid-connected VSI direct power control functionalities, as recommended in IEEE Std. 1547.2018 subsection 5.3 [15], to assist DER reactive power control. The DPC-VSI impact on grid stability under stiff, weak, and ultra-weak grid conditions are also evaluated and compared with the conventional vector current control (VCC) technique. It is expected that the control methods discussed in this paper will be beneficial in numerous VSI-grid penetrations, necessitating high dynamic and steady-state performance alongside efficient operation.

II. System Modeling and Analysis

Fig. 1 depicts the architecture of a grid-tied three-phase voltage source inverter system, which is composed of five primary elements: a DC link that could be connected to

renewable energy sources, a three-phase VSI, a DPC unit, a filtering mechanism R_f *and* L_f, and a grid source. The performance of the proposed DPC scheme is assessed through comparison with the traditional VCC technique, as represented in the models from [16] and illustrated in Fig. 2. The DC link and network parameters used in this work is shown in Table 1.

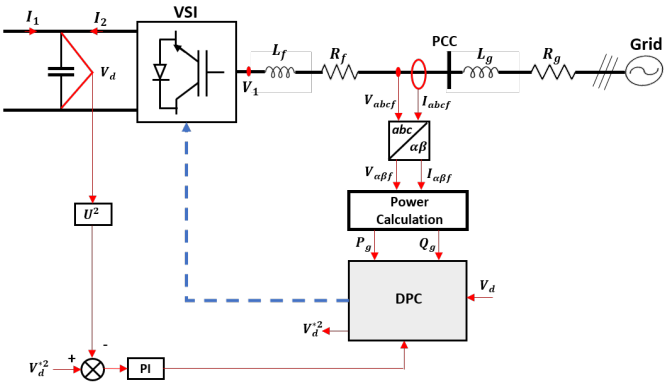

Fig. 1. Schematic diagram of the proposed DPC-VSI grid connected system.

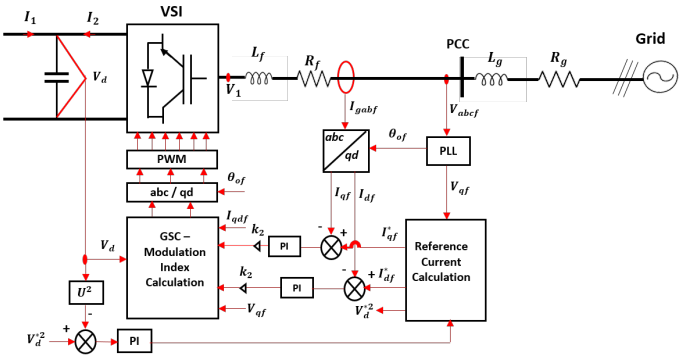

Fig. 2. Conventional VCC schematic diagram for VSI-grid penetration.

TABLE I
SYSTEM PARAMETERS

DC Link and Network Parameters			
P_1	10 kW	V_d	800 V
L_f / R_f	100 μH / 10.32 mΩ	C_d	10 mF
V_g	380$\angle$0°	ω_e	377 rad/s
R_g	0.179056 Ω	L_g	1.553581 mH

A. VSI Modeling

In this subsection, the dynamic model of the VSI in a stationary reference frame is presented. From Fig. 1, the following VSI output dynamic equations are determined:

$$pi_{\alpha\beta g} = \frac{V_{\alpha\beta 1}}{L} - \frac{R}{L} i_{\alpha\beta g} - \frac{V_{\alpha\beta g}}{L} \tag{1}$$

Where $L = L_f + L_g$, $R = R_f + R_g$, $i_{\alpha\beta g}$ = $i_{\alpha\beta f}$ and p is differential operator, $\left(p = \frac{d}{dt}\right)$. Also, assume an ideal network, the grid voltage in $\alpha\beta$ reference frame includes [16]:

$$\Rightarrow V_{\alpha\beta g} = |V_g| \left[\cos\left(\omega_e + \theta_0\right) - j sin\left(\omega_e + \theta_0\right)\right]$$

$$\therefore pV_{\alpha\beta g} = \omega_e V_{\beta g} - j\omega_e V_{\alpha g} \tag{2}$$

Also, $S_g = \frac{3}{2} V_{\alpha\beta g}\ i^*_{\alpha\beta g}$

By differentiating S_g and substituting (1) and (2), the instantaneous complex power model is obtained as follows:

$$pS_g = \frac{3}{2L}\left(V_{\alpha 1}V_{g\alpha} + V_{\beta 1}V_{g\beta} - |V_g|^2\right) - \frac{R}{L}P_g + \omega_e Q_g + \ldots$$
$$j\left[\frac{3}{2L}\left(V_{\alpha 1}V_{g\beta}\ + V_{\beta 1}V_{g\alpha}\right) - \frac{R}{L}Q_g - \omega_e P_g\right] \tag{3}$$

From (3), let the VSI dynamic inputs for active and reactive power be represented as follows:

$$U_{\text{pg}} = V_{\alpha 1}\ V_{\alpha g} + V_{\beta 1}\ V_{\beta g} - |V_g|^2 \tag{4}$$

$$U_{\text{Qg}} = V_{\alpha 1}V_{g\beta} - V_{\beta 1}V_{\alpha g} \tag{5}$$

Substitute (4-5) into (3) and decouple the complex power:

$$\Rightarrow U_{Pg} = \frac{2L}{3}\left[\left(p + \frac{R}{L}\right)P_g - \omega_e Q_g\right]$$

$$U_{Qg} = \frac{2L}{3}\left[\left(p + \frac{R}{L}\right)Q_g + \omega_e P_g\right]$$

Let: $\sigma_{\text{Pg}} = \left(p + \frac{R}{L}\right)P_g$, $\sigma_{\text{Qg}} = \left(p + \frac{R_g}{L}\right)Q_g$, and $k_g = \frac{2L}{3}$

$$\therefore U_{Pg} = k_g\sigma_{Pg} - k_g\omega_e Q_g \quad \text{and} \quad U_{Qg} = k_g\sigma_{Qg} + k_g\omega_e P_g$$

By solving (4) and (5) simultaneously, the VSI output voltage is expressed as:

$$V_{\beta 1} = \frac{U_{\text{pg}}V_{\beta g} - U_{\text{Qg}}V_{\alpha g}}{|V_g|^2} + V_{\beta g} \tag{6}$$

$$V_{\alpha 1} = \frac{U_{\text{pg}}V_{\alpha g} + U_{\text{Qg}}V_{\beta g}}{|V_g|^2} + V_{\alpha g} \tag{7}$$

B. DC Link Dynamic Modeling

From Fig. 1, the model for the DC link constant voltage control is deduced as follows:

$$C_d pV_{\text{d}} = I_1\ -\ I_2 \tag{8}$$

By multiplying both sides of (8) by V_{d}, the dc link voltage is obtained in terms of VSI active power, obtained as follows:

$$\frac{C_d}{2} pV_{\text{dc}}^2 = \ (P_1\ -\ P_g) \tag{9}$$

III. CONTROLLER DESIGN

A. VSI-DPC Design

In this section, the VSI-DPC is designed to regulate the grid power injection/absorption. Fig. 3 depicts the designed DPC, which utilizes PI controllers and feed-forward loop controls for the decoupled active and reactive power control. The decoupled active power controller can be derived from (3) - (5):

$$\Rightarrow pP_g = \omega_e Q_g - \frac{R_g}{L}P_g + \frac{3}{2L}U_{\text{pg}}$$

$$\Rightarrow U_{\text{pg}} = \frac{2L}{3}\left(pP_g + \frac{R}{L}P_g\right) - \frac{2L}{3}\omega_e Q_g$$

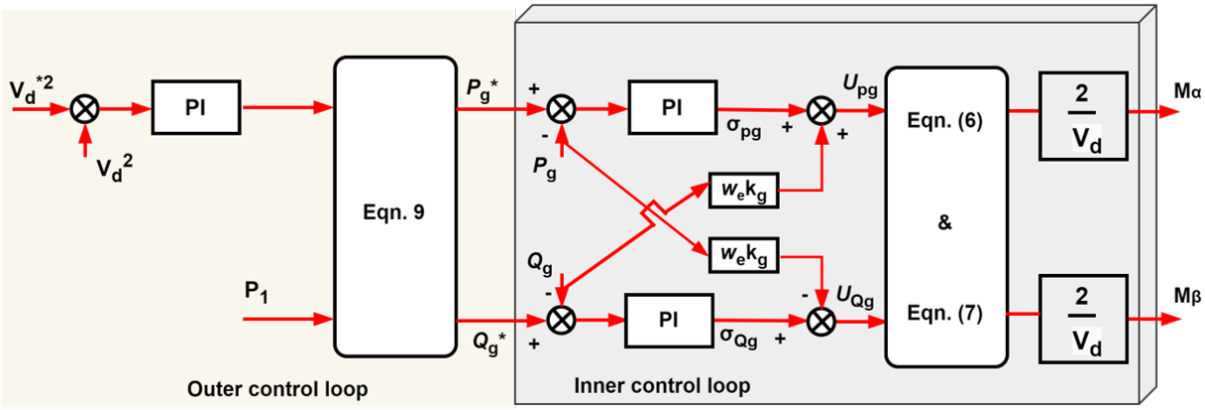

Fig. 3. DPC-VSI design for effective grid power injection.

Let, $k_{g_p} = \frac{2L}{3}$.

$\Rightarrow U_{\text{pg}} = -k_{g_p}\omega_e Q_g + k_{g_p}\left[pP_g + \frac{R}{L}P_g\right]$

Also, let, $\sigma_{\text{pg}} = pP_g + \frac{R}{L}P_g = k_{g_p}\left(P_g^* - P_g\right)$

$\Rightarrow k_{g_p}P_g^* = (p + \frac{R_g}{L} + k_{g_p})P_g$

$\Rightarrow \frac{P_g}{P_g^*} = \frac{k_{g_{pp}}\left(1+\frac{k_{gpi}}{pk_{g_{pp}}}\right)}{p\left(1+\frac{R_g}{pL}\right)+k_{g_{pp}}\left(1+\frac{k_{gpi}}{pk_{g_{pp}}}\right)}$

Assume, $\frac{R}{\rho L} = \frac{k_{gpi}}{\rho k_{g_{pp}}} \rightarrow k_{g_pi} = \frac{R}{\rho L}\, k_{g_{pp}}$

$$\Rightarrow \frac{P_g}{P_g^*} = \frac{k_{g_{pp}}}{p + k_{g_{pp}}} \tag{10}$$

From (10), let the poles = $-k_{g_{pp}}$, and the bandwidth defined as: $\alpha = k_{g_{pp}}$

$$\therefore k_{g_pi} = \frac{R_g}{L_g}\alpha \quad \& \quad k_{g_{pp}} = \alpha \tag{11}$$

The decoupled reactive component from (3):
$\Rightarrow pQ_g = -\omega_e P_g - \frac{R}{L}Q_g + \frac{3}{2L}U_{\text{Qg}}$,

$U_{\text{Qg}} = \frac{2L}{3}\left(pQ_g + \frac{R}{L}Q_g\right) + \omega_e P_g * \frac{2L}{3}$

Let, $k_{Q_g} = \frac{2L}{3}$

$\therefore U_{\text{Qg}} = k_{Q_g}\left(pQ_g + \frac{R}{L}Q_g\right) + k_{Q_g}\omega_e P_g$

Let, $\sigma_{Q_g} = pQ_g + \frac{R}{L}Q_g = k_{Q_g}\left(Q_g^* - Q_g\right)$

$\therefore k_{Q_g}Q_g^* = \left(p + \frac{R}{L} + k_{Q_g}\right)Q_g$,

$\Rightarrow \frac{Q_g}{Q_g^*} = \frac{k_{Q_g P}\left(1+\frac{k_{Q_g i}}{pk_{Q_g p}}\right)}{p\left(1+\frac{R}{pL}\right)+k_{Q_g p}\left(1+\frac{k_{Q_g i}}{pk_{Q_g p}}\right)}$

Let, $\frac{R}{pL} = \frac{k_{Q_g i}}{pk_{Q_g p}} \rightarrow k_{Q_g} i = \frac{R}{L}k_{Q_g p}$

$$\frac{Q_g}{Q_g^*} = \frac{k_{Q_g p}}{p + k_{Q_g p}} \tag{12}$$

From (12), let the poles = $-k_{Q_g p}$ and bandwidth: $\alpha = k_{Q_g p}$

$$\therefore \quad k_{Q_g i} = \frac{R}{L}\alpha \quad \& \quad k_{Q_g p} = \alpha \tag{13}$$

Fig. 3 shows the designed DPC-VSI technique considering equations (1) - (12).

B. DC Link Voltage Controller Design

In this sub-section, the DC link voltage controller is designed to ensure fast and effective control of the VSI instantaneous active and reactive power. From (9), Let:

$$\sigma_v = \frac{C_d}{2}pV_{\text{d}}^2 = k_v(V_{\text{d}}^{*2} - V_{\text{dc}}^2) \tag{14}$$

From (14), the transfer function can be deduced as follows:

$$\frac{V_{\text{d}}^2}{V_{\text{d}}^{*2}} = \frac{k_v}{\frac{C_d}{2}p + k_v} = \frac{1}{1 + \frac{C_d}{2k_v}p} \tag{15}$$

From (15), let the poles = $-\frac{2k_v}{C_d}$ and bandwidth, $\alpha = \frac{2k_v}{C_d}$.
Where, $k_v = \frac{C_d}{2}\alpha \equiv k_{\text{vp}} + \frac{k_{\text{vi}}}{p}$

$$k_{\text{vp}} = \frac{C_d}{2}\alpha \text{ and } k_{\text{vi}} = 0 \tag{16}$$

Moreover, the outer and inner loop controller parameters are shown in Table 2.

TABLE II
SYSTEM PARAMETERS

k_{vp}	10	k_{vi}	0
$k_{g_{pp}}$	167.88	k_{g_pi}	6999.63
$k_{Q_g p}$	167.88	$k_{Q_g i}$	6999.63

C. Stability Analysis

The network's parasitic components considerably influence the stability of a grid-connected VSI system. Consequently, this section demonstrates how changes in grid parameters impact the stability and dynamic response of the investigated VSI-grid network. As mentioned in [17], the rigidity of a grid

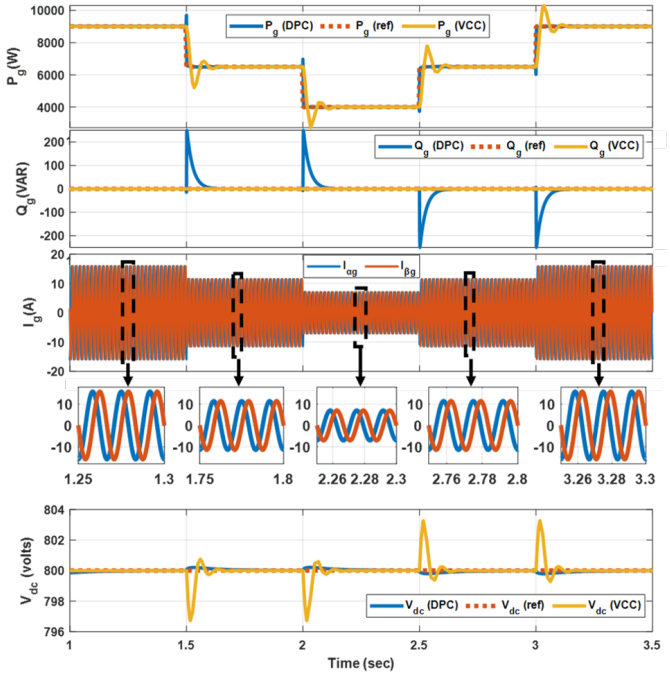

Fig. 4. VSI-grid constant VAR control transient performance comparison of DPC and VCC at varying reference power conditions.

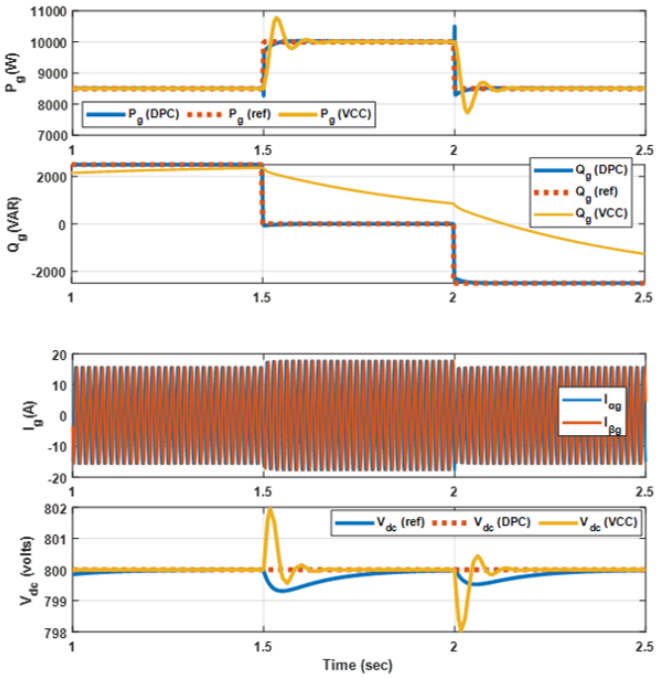

Fig. 5. VSI-grid PQ control performance comparison of DPC and VCC.

at the PCC is commonly characterized by the short-circuit ratio (SCR). In this study, SCR is computed as the proportion of the grid's short-circuit capacity at the PCC to the rated power of the VSI, which is presented in [18] [19] as:

$$SCR = \frac{V_{pcc,\ nom}^2}{P_{rated}\ |Z_{grid}|} \tag{17}$$

IV. Results and Discussion

To assess the dynamic performance of the grid-connected VSI for enhanced performance, the model represented by equations (1)-(9) has been simulated in accordance with IEEE Std 1547-2018 subsection 5.3, which pertains to the DER active-power and reactive-power characteristic requirements. Taking into account a network operator-selected set-point of 10000 W at various step changes and curtailment. Fig. 4 shows the steady-state and transient performance of DPC and VCC schemes in delivering grid power at constant reactive power mode. It can be noted that the DPC's transient response and steady-state performance are not substantially impacted by the variation in reference power, especially concerning active power and DC link voltage levels, in comparison to the conventional VCC. The overshoot observed during abrupt step changes in DPC reactive power is attributable to the change in power flow direction on the VSI, which results from reference power step changes.

Fig. 5 presents the dynamic response of the VSI-grid model under PQ control mode. The performance of the DPC and VCC models is assessed under abrupt changes in VSI

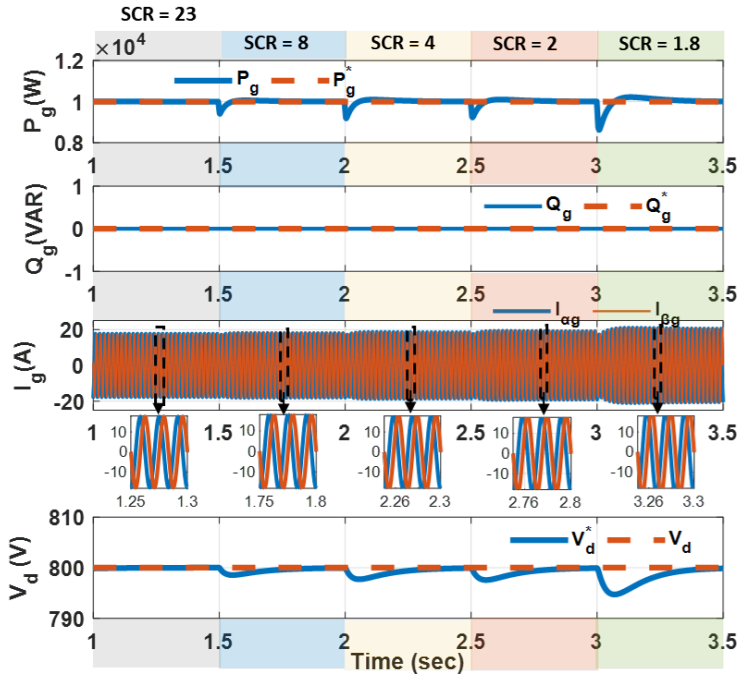

Fig. 6. Performance of DPC and VCC under different grid conditions.

reference power, transitioning from overexcited dead-band to under-excited operating modes. The results indicate that the DPC exhibits a more rapid dynamic response in comparison to the VCC model. Fig. 6 shows the VSI-DPC performance under different SCR values. At the beginning of the simulation, the VSI is connected to a stiff grid with an SCR value of 23. The grid impedance is incremented in five stages at 0.5-sec intervals to represent the transition from a stiff grid to an ultra-weak grid mode. The results reveal that the DPC demonstrates robustness and effective performance under various grid conditions.

V. Conclusion

This paper investigates approaches to improve the performance of grid-connected VSI systems. A two-phase stationary transformation scheme has been used to model the proposed VSI-grid system. The dynamic and steady-state models developed are derived directly from the network parameters. To effectively control the VSI-grid power injection, a direct power controller has been designed in this paper. The simulation results show that the DPC has a fast transient response and lesser harmonics during steady-state operations. Also, the DPC-VSI performance under weak grid conditions has been evaluated. However, the findings and discussions presented herein are expected to benefit researchers, engineers, and industry professionals working on VSI-grid integration and control strategies for modern power systems.

References

[1] J. Hashimoto, T. S. Ustun, M. Suzuki, S. Sugahara, M. Hasegawa, and K. Otani, "Advanced grid integration test platform for increased distributed renewable energy penetration in smart grids," *IEEE Access*, vol. 9, pp. 34 040–34 053, 2021.

[2] X. Liang, "Emerging power quality challenges due to integration of renewable energy sources," *IEEE Transactions on Industry Applications*, vol. 53, no. 2, pp. 855–866, 2017.

[3] J. M. Guerrero, F. Blaabjerg, T. Zhelev, K. Hemmes, E. Monmasson, S. Jemei, M. P. Comech, R. Granadino, and J. I. Frau, "Distributed generation: Toward a new energy paradigm," *IEEE Industrial Electronics Magazine*, vol. 4, no. 1, pp. 52–64, 2010.

[4] A. B. Shitole, H. M. Suryawanshi, G. G. Talapur, S. Sathyan, M. S. Ballal, V. B. Borghate, M. R. Ramteke, and M. A. Chaudhari, "Grid interfaced distributed generation system with modified current control loop using adaptive synchronization technique," *IEEE Transactions on Industrial Informatics*, vol. 13, no. 5, pp. 2634–2644, 2017.

[5] N. Kumar, I. Hussain, B. Singh, and B. K. Panigrahi, "Implementation of multilayer fifth-order generalized integrator-based adaptive control for grid-tied solar pv energy conversion system," *IEEE Transactions on Industrial Informatics*, vol. 14, no. 7, pp. 2857–2868, 2018.

[6] M. Ricco, P. Manganiello, E. Monmasson, G. Petrone, and G. Spagnuolo, "Fpga-based implementation of dual kalman filter for pv mppt applications," *IEEE Transactions on Industrial Informatics*, vol. 13, no. 1, pp. 176–185, 2017.

[7] S. Deo, C. Jain, and B. Singh, "A pll-less scheme for single-phase grid interfaced load compensating solar pv generation system," *IEEE Transactions on Industrial Informatics*, vol. 11, no. 3, pp. 692–699, 2015.

[8] N. Mahmud, A. Zahedi, and A. Mahmud, "A cooperative operation of novel pv inverter control scheme and storage energy management system based on anfis for voltage regulation of grid-tied pv system," *IEEE Transactions on Industrial Informatics*, vol. 13, no. 5, pp. 2657–2668, 2017.

[9] P. E. Kakosimos, A. G. Kladas, and S. N. Manias, "Fast photovoltaic-system voltage- or current-oriented mppt employing a predictive digital current-controlled converter," *IEEE Transactions on Industrial Electronics*, vol. 60, no. 12, pp. 5673–5685, 2013.

[10] A. K. Singh and B. C. Pal, "Decentralized dynamic state estimation in power systems using unscented transformation," *IEEE Transactions on Power Systems*, vol. 29, no. 2, pp. 794–804, 2014.

[11] H. Kong, J. He, Y. Liu, P. Cheng, and J. Ma, "Improved direct power control of doubly fed induction generator without phase-locked loop," in *2020 IEEE Sustainable Power and Energy Conference (iSPEC)*, 2020, pp. 199–204.

[12] M. Ahmed, M. Abdelrahem, I. Harbi, and R. Kennel, "Evaluation of predictive direct current and direct power control for grid-connected pv systems," in *2020 5th IEEE Workshop on the Electronic Grid (eGRID)*, 2020, pp. 1–6.

[13] M. S. Sadabadi, M. Sharifzadeh, M. Mehrasa, S. Bacha, and K. Al-Haddad, "Convex optimization-based vector current control design for grid-connected packed e-cell inverters," in *2021 IEEE Energy Conversion Congress and Exposition (ECCE)*, 2021, pp. 2607–2612.

[14] Z. Chen, C. Wang, J. Chen, H. Xue, and J. Wang, "Model predictive direct power control method of energy storage converter in micro-grid," in *2019 IEEE 10th International Symposium on Power Electronics for Distributed Generation Systems (PEDG)*, 2019, pp. 321–326.

[15] "Ieee standard for interconnection and interoperability of distributed energy resources with associated electric power systems interfaces," *IEEE Std 1547-2018 (Revision of IEEE Std 1547-2003)*, pp. 1–138, 2018.

[16] Y. Gui, X. Wang, F. Blaabjerg, and D. Pan, "Control of grid-connected voltage-source converters: The relationship between direct-power control and vector-current control," *IEEE Industrial Electronics Magazine*, vol. 13, no. 2, pp. 31–40, 2019.

[17] L. Zhang, L. Harnefors, and H.-P. Nee, "Interconnection of two very weak ac systems by vsc-hvdc links using power-synchronization control," *IEEE Transactions on Power Systems*, vol. 26, no. 1, pp. 344–355, 2011.

[18] C. M. Emeghara, S. M. Mahajan, and A. Arzani, "Direct power control of a surface-mounted permanent magnet synchronous generator wind turbine for offshore applications," *IEEE Access*, vol. 11, pp. 62 409–62 423, 2023.

[19] O. Damanik, O. C. Sakinci, G. Grdenic, and J. Beerten, "Evaluation of the use of short-circuit ratio as a system strength indicator in converter-dominated power systems," in *2022 IEEE PES Innovative Smart Grid Technologies Conference Europe (ISGT-Europe)*, 2022, pp. 1–5.